

Bifurcations of a DFB Laser with Short Optical Feedback: Numerical Experiment

Nikolay Korneyev^a, Mindaugas Radžiūnas^b, Hans Jürgen Wünsche^a, and Fritz Henneberger^a

^a Humboldt-Universität zu Berlin, Institut für Physik, Invalidenstr. 110, 10115 Berlin, Germany

^b Weierstraß-Institut für Angewandte Analysis und Stochastik, Mohrenstr. 39, 10117 Berlin, Germany

ABSTRACT

We have applied a comprehensive simulation tool for multisection DFB lasers to systematically investigate bifurcations caused by combining a single mode DFB laser with a feedback section. Strength and phase of the optical feedback are considered as main bifurcation parameters. The recording of output power, optical and power spectra and carrier density yield evidence of fold bifurcations of stationary states as well as subcritical and supercritical Hopf bifurcations towards self-pulsations. Furthermore, a homoclinic bifurcation is detected and indications for a fold of limit cycles are observed in qualitative agreement with a bifurcation diagram very recently calculated with path following techniques⁷ under simplifying assumptions. The present simulations show that these bifurcations are stable with respect to these approximations. They offer a method how the bifurcations can be determined experimentally.

Keywords: semiconductor laser, optical feedback, bifurcation, distributed feedback, short-delay limit

1. INTRODUCTION

An ideal single mode semiconductor laser is a type B laser: it has a stable output and it reacts to external perturbations with well damped relaxation oscillations. To get a more complex dynamics, additional interactions are required (examples: feedback, optical injection, saturable absorbers, external modulation, multisection structures, coupling to other lasers). In particular, optical feedback can cause hysteresis effects, regular self-pulsations but also chaotic output. In order to control these effects it is important to know the parameter regions where the different phenomena appear and how they can be addressed in experiments. Knowledge of the position and of the nature of the bifurcations, which form the borders of these regions, provides this information.

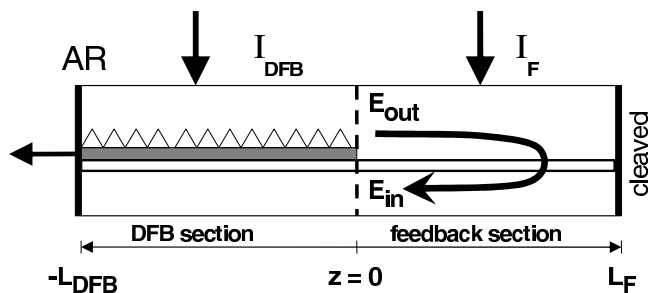


Figure 1. Scheme of a DFB laser with integrated feedback cavity.

First studies of optical feedback effects were done in the context of unwanted perturbations by external reflexions from fibre ends (see Ref.¹). Later, optical feedback by external reflections has been used in a controlled manner to prepare light sources for chaotic communication.² These cases correspond to the long delay limit, i.e., the round trip time τ of the light from the laser to the reflector and back is large compared with the period T_{ro} of the relaxation oscillations.

Here we study the opposite short-delay limit. In particular, we consider a single-mode DFB laser integrated with a passive feedback section as sketched in Fig. 1. The feedback can be characterized by the relation

$$E_{in}(t) = K \exp(i\varphi) E_{out}(t - \tau) \quad (1)$$

H.J.Wünsche is also with Fraunhofer-Institut Nachrichtentechnik Heinrich-Hertz-Institut, Einsteinufer 37, 10587 Berlin, Germany

between the amplitudes E_{out} emitted by the laser and E_{in} fed back to it. The real numbers K and φ are strength and phase of the feedback, respectively. The delay time τ is determined by the length L_F of the feedback section. In realized devices of this type, L_F is only few hundred μm long.⁹ These lengths correspond to less than 10 ps round trip time, which is indeed small compared to typically few hundred ns relaxation oscillation period.

First theoretical investigations of the short delay were given by Tager and Petermann.³ Starting from the Lang-Kobayashi model⁴ they recognized the possibility of high-frequency self-pulsations due to the beating of a mode and an antimode. Later, this prediction has been confirmed by a detailed mathematical analysis of the LK equations by Emeux et al.⁵ and by Wolfrum and Turaev.⁶ Besides confirming the results of Refs.^{3,5} for the mode-beating SP, Ref.⁶ has shown the appearance of a further type of self-pulsations with much lower frequencies at lower feedback strength. In difference to the aforementioned work, Sieber⁷ has very recently presented an analysis of short delayed feedback that bases not on the LK equations but on the travelling wave equations (TWE). This approach is better suited for the cases of short and strong feedback because it resolves the spatial structure of the optical field within the full compound cavity. The bifurcations of stationary states of a laser with short optical feedback obtained on base of the LK equations^{5,6} were qualitatively reestablished. Furthermore, the analysis of Sieber yielded a rich world of additional bifurcations of the two types of self-pulsations, among them Torus- and homoclinic bifurcations.

The tori are probably closely related to the regular pulse packages discovered recently with an intermediate-delay configuration ($\tau \approx T_{ro}$).⁸ The presence of a homoclinic bifurcation has been used to prepare excitability of a semiconductor laser⁹ (for a generalizing theoretical analysis see Ref.¹⁰). However, no systematic experimental verification of the complete bifurcation scenario exists yet. The present paper describes a corresponding numerical experiment. We have reinvestigated the bifurcation scenario of Sieber by applying a comprehensive simulation tool for multisection DFB lasers. The underlying model is described in Section 2 and it avoids the simplifying assumptions of Sieber (two-mode approximation and neglect of gain dispersion, nonlinear gain suppression, and longitudinal spatial hole burning). One aim of our investigation is to find out how stable the bifurcation scenario is with respect to these simplifications. The second aim is to develop and to test methods for detecting and identifying different bifurcations being applicable in real experiments. In Section 3 we demonstrate that recording of output power, optical spectra, power spectra, and average carrier density allows to identify fold bifurcations of stationary states, subcritical and supercritical Hopf bifurcations, as well as a homoclinic bifurcations. Furthermore, indications for a fold of limit cycles are observed in qualitative agreement with Sieber's bifurcation diagram. The paper ends with conclusions in Section 4.

2. MODEL

The standard treatment of lasers with delayed feedback is due to the Lang-Kobayashi equations.⁴ However, in the present case, the feedback is not weak, nor is the feedback section much longer than the laser section. Instead, a spatio-temporal structure develops across the entire device, which has to be properly accounted for. An adequate description is given by the travelling wave equations (TWE)

$$\left(-\frac{i}{v_g} \frac{\partial}{\partial t} \mp i \frac{\partial}{\partial z} + \beta - i \frac{\alpha_0}{2} \right) E_{\pm} + \kappa E_{\mp} = 0 \quad (2)$$

for the slowly varying amplitudes $E_+(z,t)$ and $E_-(z,t)$ of the forward and backward travelling waves, respectively. The boundary conditions are $E_+(-L_{DFB},t) = 0$ at the anti-reflection (AR) coated DFB facet and $E_-(L_F,t) = rE_+(L_F,t)$ at the cleaved facet of the feedback section. By proper normalization, $|E(z,t)|^2 = |E_+|^2 + |E_-|^2$ is the local photon density. β describes the linear propagation properties of the fundamental transverse mode of the internal waveguide at a central optical frequency ω_0 (corresponding to the wavelength $\lambda_0 = 1.54$ nm throughout the paper). The counterpropagating waves are mutually coupled with the DFB coupling strength κ . The parameter models for the two sections are different. In the passive feedback section, κ disappears and the propagation parameter is a constant that we express by the round trip phase shift φ over the sectional length L_F and an optical loss coefficient α as

$$\beta = -\frac{\varphi}{2L_F} - i \frac{\alpha}{2} \quad (\text{feedback section}). \quad (3)$$

In the active DFB section, the model for the propagation parameter is

$$\beta = -i \frac{\alpha}{2} + (i + \alpha_H) \frac{g}{2} - iD \quad (\text{active section}). \quad (4)$$

Table 1: Parameter values

		DFB section	feedback section	unit
L	length	220	250	μm
r	facet amplitude reflectivity	0	K (varied)	
c/v_g	group velocity index	3.8	3.8	
κ	coupling coefficient	180	–	cm^{-1}
α	optical losses	25	0	cm^{-1}
α_H	Henry factor	–5	–	
g'	differential gain	5	–	10^{-17}cm^2
n_{tr}	transparency carrier density	1.3	–	10^{18}cm^{-3}
ε	gain compression factor	1	–	10^{-18}cm^3
τ_s	linear carrier lifetime	1	–	ns
V	volume of active zone	9.9	–	10^{-11}cm^3
I	current injection, DFB section	50	–	mA
U'_F	differential Fermi voltage	$1.2 * 10^{-25}$	–	10^{-20}V/cm^3
R_s	series resistivity	5	–	Ω
\bar{g}	Lorentzian gain amplitude	100	–	cm^{-1}
$\bar{\omega}$	gain peak detuning	–2.82	–	10^{12}s^{-1}
$2\bar{\gamma}$	FWHM of gain curve	3.18	–	10^{12}s^{-1}

α_H is the linewidth enhancement factor. The spectral gain maximum is assumed to depend on carrier density n and photon density $|E|^2$ according to

$$g(n, \varepsilon |E|^2) = \frac{g'(n - n_{tr})}{1 + \varepsilon |E|^2} \quad (5)$$

with the gain slope g' and the nonlinear saturation coefficient ε . The gain dispersion contribution \mathcal{D} to the propagation constant β in Equ. (4) is a linear operator determined by

$$\mathcal{D}E^\pm \stackrel{\text{def}}{=} \frac{\bar{g}}{2}(E^\pm - p^\pm) \quad \text{and} \quad -i\partial_t p^\pm = -\bar{\gamma}(E^\pm - p^\pm) + \bar{\omega}p^\pm. \quad (6)$$

This oscillator model for the polarization yields a Lorentzian-shape gain dispersion.¹¹ Height, width, and peak position relative to ω_0 of the Lorentzian are determined by the parameters \bar{g} , $\bar{\gamma}$, and $\bar{\omega}$, respectively. The parameter values of the table support stable lasing of the short-wave DFB mode.

The evolution of the carrier densities in the DFB is described by the rate equation

$$\partial_t n = J(z, t) - \frac{n}{\tau_s} - v_g \Re[E^*(g + 2\mathcal{D})E], \quad (7)$$

τ_s : carrier life time. In contrast to our former model,¹² the stimulated recombination (last term) is not averaged over one section. Hence, we allow now for densities varying also with z . This effect is usually called longitudinal spatial hole burning (LSHB). A quantitative description of LSHB requires to take into account the current self-distribution (CSD): the injection current density becomes also inhomogeneous in order to ensure a constant voltage along the electrical contact.^{13–16} To this purpose, we use the model

$$J(z, t) = \frac{I}{eV} - \frac{U'_F}{eVR_s}(n(z, t) - \bar{n}(t)) \quad (8)$$

for the injection rate of Equ. (7). The first term determines the average injection rate by the constant injection current I and the active volume V of the DFB section. The second term is the CSD contribution linearized with respect to the deviation of the density from its spatial mean value $\bar{n}(t)$ beneath a given electrical contact. The derivative of the Fermi level separation U'_F and the series resistivity R_s are treated as constant parameters.

The calculations to be presented base on the parameter values collected in Table 1, deviations will be noted. Note that g' , ε , and \bar{g} already incorporate the transverse confinement factor Γ .

3. RESULTS

In order to understand the behaviour of the system we explore the dynamics numerically in the two-parameter plane of feedback strength and feedback phase (K, φ), keeping all other parameters at the values given in the table. The procedure is similar to Refs.^{17,18}

We start with the smallest feedback strength level K and make a series of calculations with tuning the phase parameter φ in small steps from 0 to 2π and back.

For every point (K, φ) we solve the TW model in time domain until the transient stabilizes. Then we continue the calculation for another 10 ns and record the following quantities for a first characterization of the achieved attractor: minima and maxima of output power $P(t)$ at the DFB facet, dominant wavelength (highest peak of the optical spectrum from the fast Fourier transform of $E_-(t)$ at the DFB facet), and pulsation frequencies (highest peak of the power spectrum from the fast Fourier transform of $P(t)$). All these quantities can also be measured with real devices. In addition we also record the average carrier density in the DFB. This quantity is not directly measurable but is monotonously related to the measurable voltage across the contacts of the DFB section.

This procedure is repeated after changing the phase φ by one step with using the old final state as the new initial state. When plotting the recorded data versus φ (cf. Figs. 2 and 4), we detect points, where at least one of these quantities jumps or exhibits a cusp. To identify the nature of these bifurcations, a more detailed analysis of the transient or of the spectra is done if necessary (cf. Figs. 3, 5, 6, and 7).

After having finished this analysis for one phase period forward and back, K is increased by one step and the whole procedure is repeated. As upper limit for the feedback strength we take $K = 0.6$, corresponding to a lossless feedback section with the reflectivity of a cleaved facet, $R \approx 0.36$. Within this feedback interval we found 6 different types of

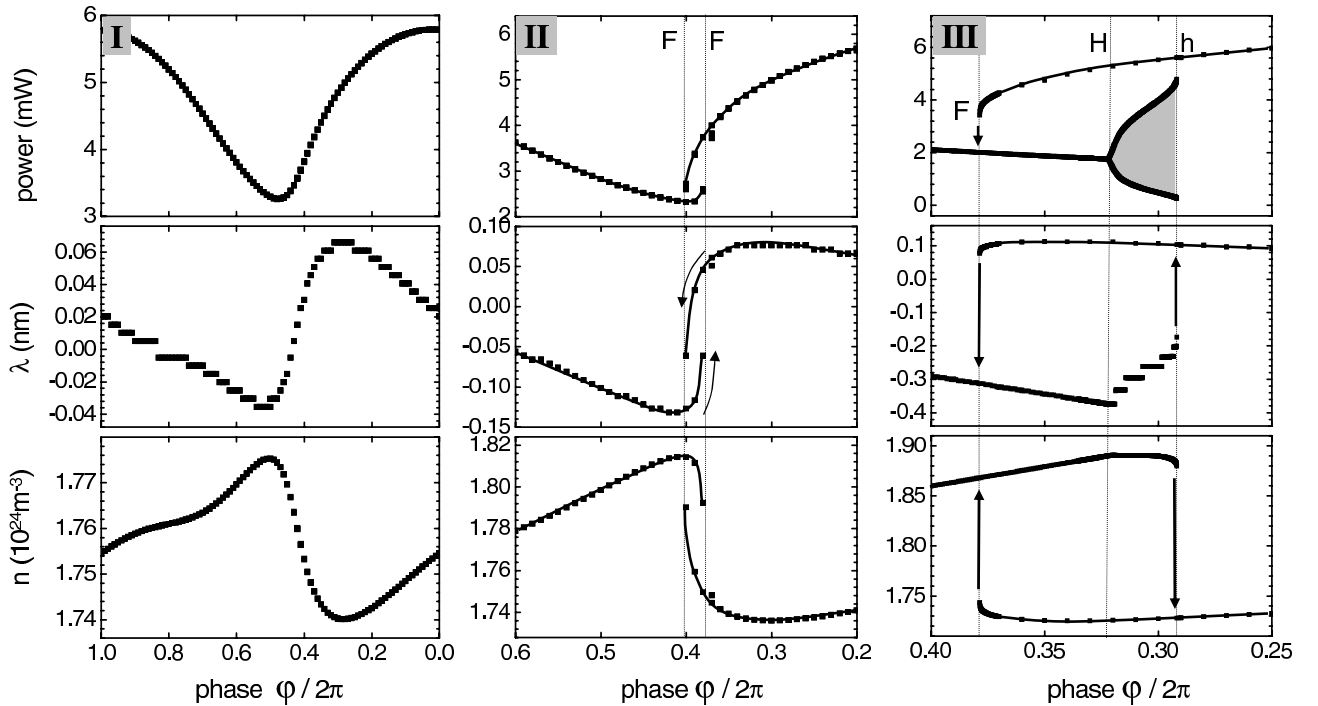


Figure 2. Dependence of measurable quantities on the feedback phase φ . The three columns of panels belong to the bifurcation scenarios I to III discussed in the text. The corresponding feedback strengths are given by $K^2 = 0.003, 0.006$, and 0.02 , respectively. First row of panels: minimum and maximum of output power during the simulation interval of time, second row: wavelength of the main peak of the optical spectrum, third row: mean carrier density in the DFB section. Dots represent calculated data, solid lines serve as a guide for the eye, arrows indicate the directions of phase change or of jumps in case of hystereses. Grey regions in the power panels indicate nonstationary output (maximum and minimum are different).

bifurcation scenarios along φ . In the following, these scenarios will be characterised in detail and finally combined in Fig. 8 to a bifurcation map in the two-parameter plane (K, φ) .

3.1. Scenario I

Column I of Fig. 2 shows results typical for the case of very weak feedback. There are no bifurcations within this scenario. Minimum and maximum output power coincide for all values of φ , i.e., the laser always exhibits continuous wave (cw) emission. Such cw states with constant $P(t)$ and $n(t)$ are usually called stationary states or equilibria although the phase of the optical amplitudes E_{\pm} is uniformly rotating.

The cyclic variation of the carrier density n with φ indicates the changing threshold due to the phase dependent interference between the light in the DFB and the wave fed back to it. It is accompanied by an according variation of the wavelength. Note that the wavelength increases much faster than it decreases. Reason is the dispersion in the phase section causing an additional phase shift that increases with decreasing wavelength. This asymmetry increases with raising K until the rising edge of the $\lambda(\varphi)$ -curve becomes vertical at $K \approx 0.077, \varphi \approx 0.39$. This codimension two bifurcation corresponds to the cusp bifurcation of Refs.^{6,7}.

3.2. Scenario II

Column II of Fig. 2 shows simulation results for a K slightly above the cusp. Jumps of all quantities are clearly observed at the two phases labelled by F . These two bifurcations merge and annihilate when going with K back through the cusp. At the left bifurcation F , all recorded quantities jump when changing the phase from right to left. Reverse, the jump is at the right F . Since all states are stationary (maximum and minimum output power coincide) and the slopes of $n(\varphi)$ and $\lambda(\varphi)$ become vertical in the respective points F , we identify these bifurcations as folds of stationary states in accordance with Refs.^{6,7}. The laser is bistable between the two folds, i.e., two stationary attractors coexist there, each one belonging to a different optical mode. The saddle branch connecting the two folds is not detected in the simulation, because only stable states can be observed.

3.3. Scenario III

Most prominent new feature of column III of Fig. 2 is the grey shaded area in the power plot. Maximum and minimum of the output power $P(t)$ differ here from each other, indicating a nonstationary state. In particular, $P(t)$ (not plotted) shows periodic self-pulsations (SP) within the full phase interval between the two bifurcations labelled with H and h . H can be identified as a Hopf bifurcation: the damping of relaxation oscillations falls to zero when approaching H from left (Fig. 3a). This Hopf bifurcation is supercritical: the SP amplitude raises smoothly beyond H and the SP frequency just right of H coincides with the relaxation oscillation frequency just left of it (Fig. 3b). Accordingly, the SP are undamped single-mode relaxation oscillations. The type of the SP is dispersive self Q-switching (DQS).^{19,20} The linear dispersion of the feedback section acts as the necessary dispersive element. When approaching the opposite end of the pulsation region, the amplitude of the SP becomes quite big and the frequency goes down towards zero, clearly indicating a homoclinic

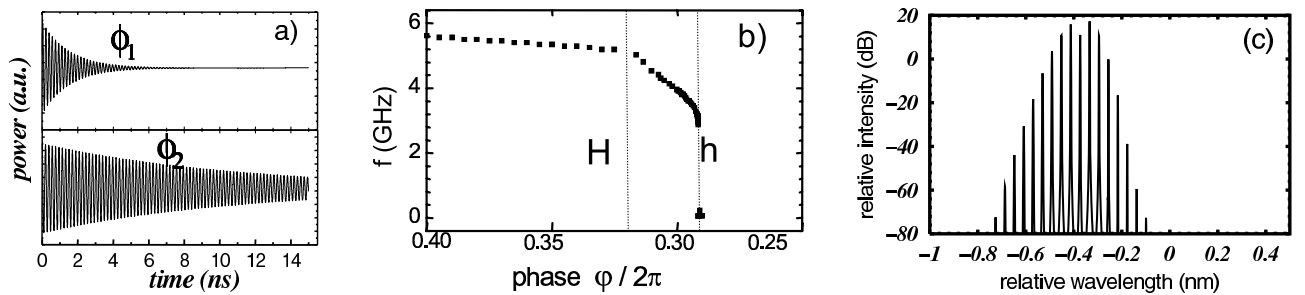


Figure 3. Characteristics of the self-pulsations in scenario III of Fig. 2. a) damped relaxation oscillations left to bifurcation H . Φ_1 : far from H , Φ_2 : close to H . b) frequency vs. φ . Left of H : relaxation oscillation. Between H and h : regular self-pulsation. The distinct decrease of f when approaching h is characteristic of a homoclinic bifurcation. c) Optical spectrum for $\varphi = 0.312$. The splitting of the single laser mode into multiple subpeaks is an effect of the amplitude and frequency modulation of the SP but not due to the participation of other modes. The separation between subsequent peaks corresponds exactly to the pulsation frequency.

bifurcation h . The stable phase orbit touches the saddle in this point. Beyond it, the system jumps to the other mode along the unstable manifold of the saddle. This happens without reaching the right fold F , which is not detected in the simulation, therefore.

The optical spectrum in Fig. 3c is typical for single-mode DQS self-pulsations. The periodic amplitude and frequency modulation causes a splitting into a comb of equidistant subpeaks. The wavelength plotted in Fig. 2 is the position of the highest subpeak. Its stepwise shift between H and h is due to changes of the spectral envelope of the subpeaks which individually keep their position.

Note that the SP appear only when changing the phase from left to right. In the reverse direction, the laser stays in the stationary state of the mode with the longer wavelength until fold F is reached and jumps down there to a stationary state of the other mode. This scenario has coexistence of two stationary states between F and H and coexistence of a stationary state and a self-pulsation between H and h .

3.4. Scenario IV

Scenario IV is drawn as first column of Fig. 4. The only qualitative difference to scenario III is the interchange of H and F . As a consequence, the laser jumps from a stationary state of one mode into a DQS self-pulsation of the other mode when crossing F from right to left. Within the dark shaded region between H and F , these self-pulsations are the only

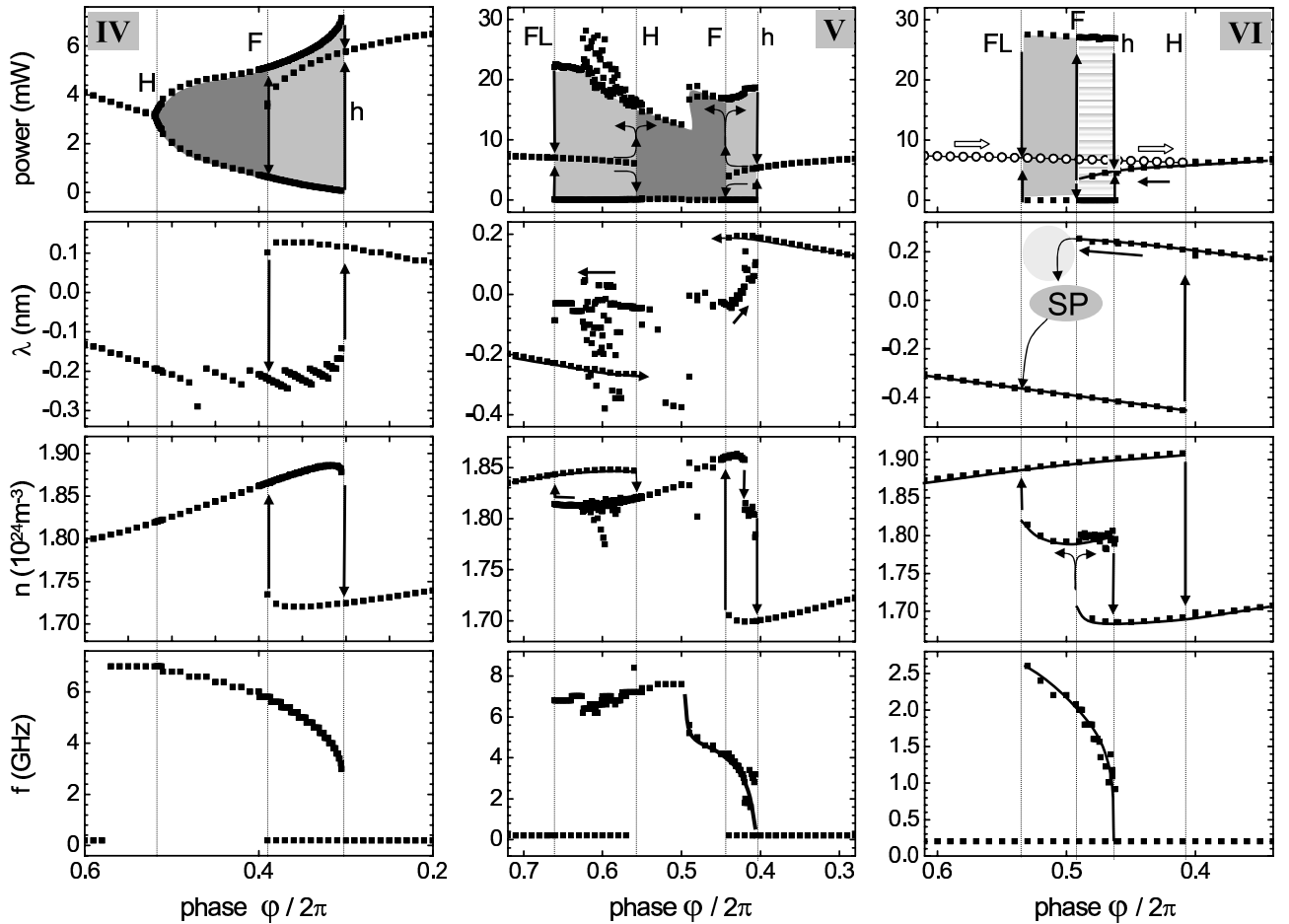


Figure 4. Dependence of measurable quantities on the feedback phase ϕ . The 3 columns are examples for the scenarios IV to VI discussed in the text. The corresponding feedback strengths are given by $K^2 = 0.03, 0.10$, and 0.18 , respectively. The lowest row of panels gives the frequencies of weakly damped relaxation oscillations or self-pulsations. The other notations are as in Fig. 2.

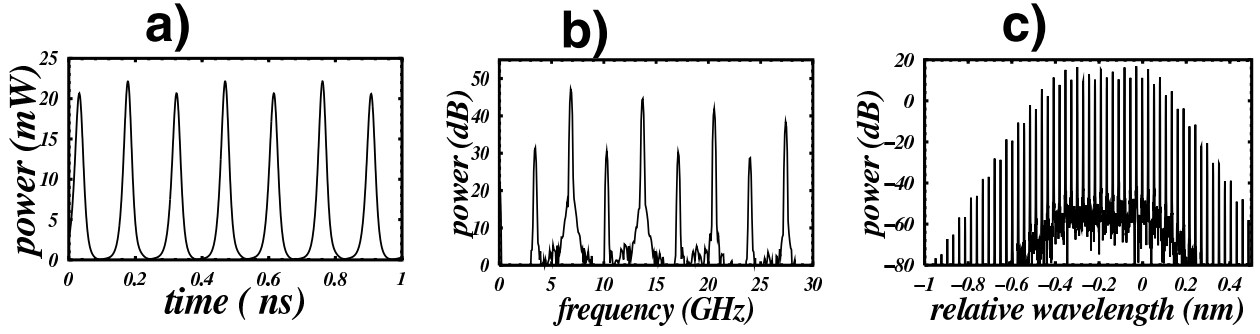


Figure 5. Characteristic example for periodic doubling of the self-pulsations in scenario V (see Fig. 4). The parameters are $\varphi = 0.645$ and $K^2 = 0.1$. a) transient: alternating pulse heights. b) power spectrum: additional small peaks exactly at half the basic frequency (which is ≈ 7 GHz) and exactly in the middle between its harmonics. c) optical spectrum: also smaller lines in the middle between the original subpeaks from before the period doubling.

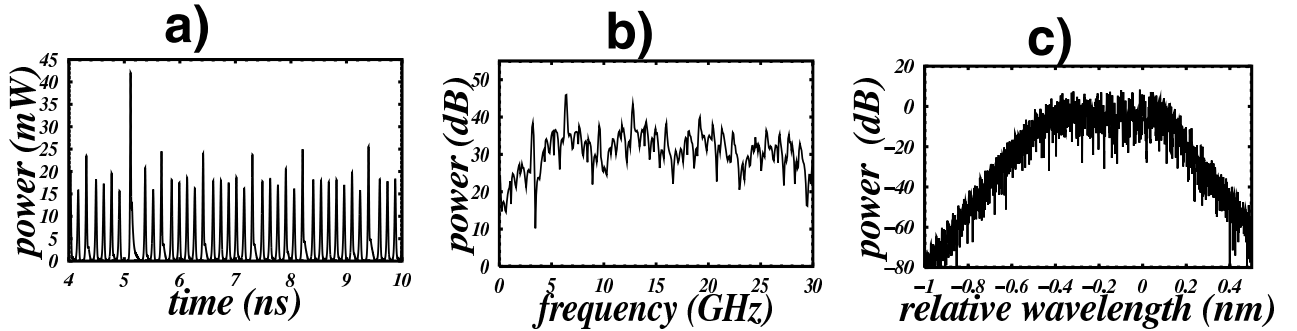


Figure 6. Characteristic example for chaotic self-pulsations in scenario V (see Fig. 4). The parameters are $\varphi = 0.63$ and $K^2 = 0.1$. a) transient: irregular peak heights and irregular pulse separations. b) power spectrum: broad noisy background with few main peaks (which are similar to Fig. 5b) on top. c) optical spectrum: noisy wide band, no splitting into distinct sublines.

attractor (detected in the simulation). The self-pulsations in the light-grey shaded region between F and h are attached only when crossing F from left.

3.5. Scenario V

In scenario V, the Hopf, Fold, and homoclinic bifurcations are observed in the same way as already in scenario IV. However, the onset of the self-pulsations is sudden when crossing H from the left stationary state, i.e., H changed its character from supercritical to subcritical. As a consequence, the pulsation survives when crossing H back to the left. The SP ends in a bifurcation labelled as FL because it should be a fold of limit cycles according to Ref..⁷ We could however not proof this assignment because the unstable cycle is not accessible in the simulation.

In contrast to scenarios III and IV, not all nonstationary states of scenario V are regular self-pulsations. They change their quality in complicated sequences of bifurcations when changing φ between FL and h . A systematic exploration of this microcosmos is not possible here. We give only examples for period doubling and chaos. The period doubling appears at $\varphi = 0.645$. It comes as a peak height modulation in $P(t)$, as an additional peak at half frequency in the power spectrum and as additional peaks in the optical spectra (Fig. 5).

In the chaotic regime at $\varphi \approx 0.6$ the peak height becomes irregular (Fig.6). The basic frequency is still observable in the power spectrum but the peaks are lower and considerably broadened. A background noise level appears. The distinct subpeak structure of the optical spectrum is lost.

Note that the plotted wavelengths of the nonstationary states vary considerably, covering a range even wider than the separation between the wavelengths of the two stationary states. This is a consequence of the wide central plateau of the envelope of the optical spectrum: already small parameter changes can cause a wide shift of the absolute maximum. In

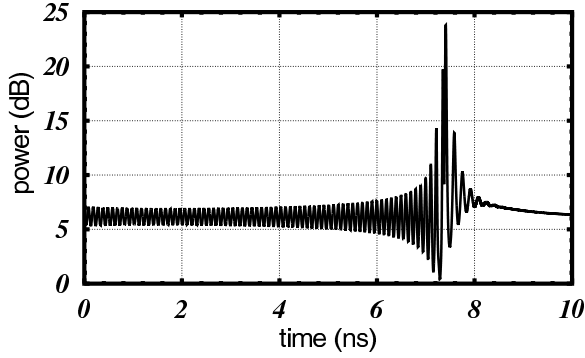


Figure 7. Transient of the mode jump just right of the Hopf bifurcation H in scenario VI (see Fig. 4). The parameters are $K = 0.42$ and $\varphi = 0.4$, which is by $\delta\varphi = 0.001$ right of H . The first part of the transient shows a small relaxation oscillation with very slowly increasing amplitude. After the amplitude exceeds a certain value, its increase accelerates and the laser relaxes quickly into the cw state of the other mode.

case of chaotic emission, the highest peak appears even at a random position within the more than 0.5 nm wide spectral band. Because it makes no sense to draw the absolute peak position in such situations, we indicate the spectral position of similar nonstationary states only symbolically in the following column VI of Fig. 4.

3.6. Scenario VI

As already in scenario V, there is again a nonstationary attractor with self-pulsations, that ends with a homoclinic bifurcation h at one edge, and with a fold of limit cycles FL at the opposite one. However, the laser jumps to this attractor only when crossing the fold F of the stationary long wave mode from right. Changing the phase parameter φ oppositely from left to right, the cw state of the short wave mode keeps stable until a bifurcation labelled with H . Because this bifurcation is far right of the end of the stable SP in h , this SP cannot be excited here. Instead, the laser jumps to stationary emission of the other mode after crossing H from left to right. When approaching H from the left, we detect relaxation oscillations with about 10 GHz frequency with decreasing damping. Thus H is a Hopf bifurcation. Fig. 7 shows a transient just right of H by $\delta\varphi = 0.001$. Initially, we observe the weakly undamped relaxation oscillations of the short-wave mode. It changes its quality when exceeding a certain amplitude and relaxes towards the other mode. H is probably a subcritical Hopf bifurcation similar to that in scenario V but only shifted right of h . This situation is sketched qualitatively in panels V and VI in the right part of Fig. 8 but Ref.⁷ offers also other possibilities. We could not clarify this ambiguity because unstable states are not observable in our simulation.

3.7. Two-parameter bifurcation diagramm

The calculations described so far for six special values of K were done on a much more dense K -grid. The results are summarised in Fig. 8 as a bifurcation diagram in the two-parameter plane φ, K . The position of the scenarios already discussed are indicated as horizontal lines. The Figure clearly shows how the transformation between the scenarios happens when increasing K . It also shows that only these 6 different scenarios exist in the regarded range of K (when taking into account only the observed bifurcations). An exception is perhaps the transition region between scenarios V and VI, where the Hopf bifurcation H crosses or touches all other bifurcations within a small part of parameter plane. A similar situation appears in the lower right corner where F , H , and h come close together. The resolution of these special constellations is however beyond the scope of this paper.

Finally, we compare Fig. 8 with Sieber's bifurcation diagram (Fig. 11 of Ref.⁷) of a simplified two-mode model. The bifurcations F, H, h, FL appear similar in both diagrams (when disregarding unstable branches also shown by Sieber). This agreement allows to draw some conclusions. First, the dynamics in the considered feedback range $K < 0.6$ is indeed essentially determined by those two modes selected by Sieber. Second, other effects neglected by Sieber (spatial hole burning, nonlinear gain saturation) do not change the quality of the dynamics. Of course, there are differences with respect to some details. Most striking one is a general shrinkage of the region with self-pulsations compared to Sieber's diagram. No SP occur below the cusp, the Hopf-curve is shifted towards higher feedback strengths, and the narrow channel with mode-beating SP at the higher part of the Hopf-branch could not be detected. Since these items also depend on the values of other parameters, a further clarification requires an experimental bifurcation analysis with real devices.

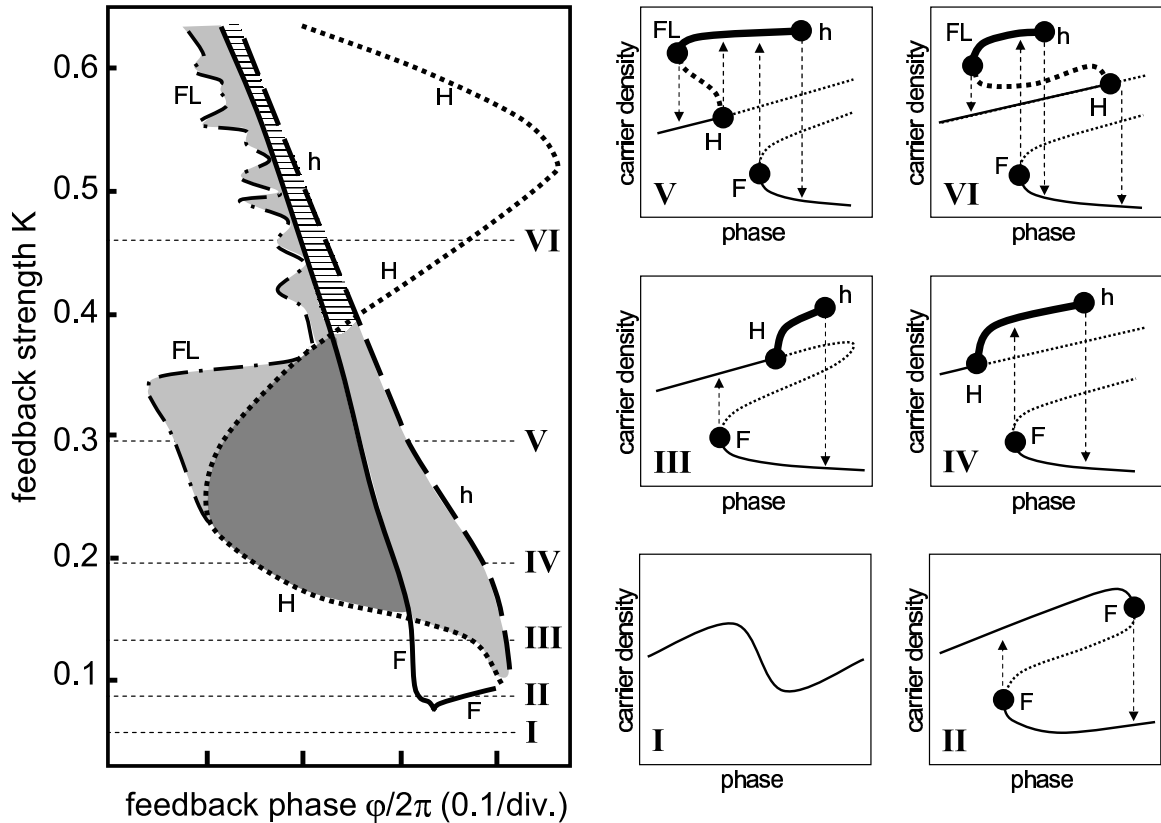


Figure 8. Calculated two-parameter bifurcation diagram. Left panel: location of the bifurcations in the plane spanned by feedback phase ϕ and strength K . Solid: fold of equilibria, dotted: Hopf, dashed: homoclinic, dash-dotted: fold of limit cycles. Dark grey areas: self-pulsations are the only attractor. Light grey areas: self-pulsations coexist with equilibria. Horizontal-dashed area: self-pulsations coexist with two different equilibria, the SP appear only when crossing the fold from right. The right panels are qualitative illustrations of the sequences of bifurcations for the six different values of K indicated in the left panel. Thin: cw states. Thick: nonstationary states.

4. CONCLUSION

Semiconductor lasers with optical feedback offer a very complex world of nonlinear dynamical scenarios. In order to control these effects it is important to know the parameter regions where the different phenomena appear and how they can be addressed in experiments. Knowledge of the position and of the nature of the bifurcations, which are the borders of these regions, provides this information. We have focussed to a DFB laser with an integrated short feedback section, regarding strength K and phase shift ϕ of the feedback as main bifurcation parameters. The bifurcations were detected by using a comprehensive simulation tool for multisection DFB lasers. Only by recording the measurable quantities output power, optical and power spectra, and mean carrier density, we could obtain evidence of fold bifurcations of stationary states, subcritical and supercritical Hopf bifurcations towards self-pulsations, and a homoclinic bifurcation. In addition, indications for a fold of limit cycles were observed. All results are in qualitative agreement with a bifurcation diagram previously calculated by Sieber with path following techniques on base of several simplifications. The results of our numerical experiment are important with two respects. First, they show that the appearance of these bifurcations is rather insensitive to the effects neglected in the previous analysis, i.e., the corresponding phenomena are a genuine property of short-feedback lasers. Second, the methods applied in the numerical experiment can be transferred to the laboratory. When measuring the corresponding quantities of real devices, it should be possible to experimentally determine and identify these bifurcations in the same way. Such experiments would give important information for a controlled application of the investigated phenomena.

The work was supported by Deutsche Forschungsgemeinschaft in frame of Sfb 555.

REFERENCES

1. K. Petermann "External Optical Feedback Phenomena in Semiconductor Lasers," *IEEE J. of Quantum Electronics* , vol. **1**, pp. 480-489, 1995.
2. Jia-ming Liu, How-foo Cheng and Shuo Tang "Synchronized Chaotic Optical Communications at High Bit Rates," *IEEE J. of Quantum Electronics* , vol. **38**, pp. 1184-1196, 2002.
3. A. Tager and K. Petermann "High Frequency Oscillations and Self-Mode Locking in Short External-Cavity Laser Diodes," *IEEE J. of Quantum Electronics* , vol. **30**, pp. 1553-1561, 1994.
4. R. Lang, K. Kobayashi, "External Optical Feedback Effects on Semiconductor Injection Laser Properties," *IEEE J. Quantum Electron.*, **16**, pp. 183-188, **16**, pp. 347-355, 1980.
5. T. Erneux , F. Rogister, A. Gavrielides, V. Kovanis "Bifurcations to mixed external cavity mode solutions for semiconductor lasers subject to optical feedback ," *Opt. Comm.* , **183**, pp. 476-477, 2000.
6. M. Wolfrum, D. Turayev, "Instabilities of Lasers with Moderately Delayed Optical Feedback", *Opt. Comm.* , **212**, pp. 127-138, 2002.
7. J. Sieber, "Numerical bifurcation analysis for multi-section semiconductor lasers", *SIAM J. of Appl. Sys.* **1**, No. 2, pp. 248-270, 2002.
8. T. Heil, I. Fischer, W. Elsässer and A. Gavrielides, "Dynamics of Semiconductor Lasers Subject to Delayed Optical Feedback: The short cavity regime", *Phys. Rev.Letts.*, **24**, pp. 243901-1 - 4, 2001.
9. H.J. Wünsche, O. Brox, M. Radziunas and F. Henneberger, "Excitability of a Semiconductor Laser by a Two-Mode Homoclinic Bifurcation," *Phys.Rev.Lett.* **88**, 023901 (2002)
10. B. Krauskopf, K. Schneider, J. Sieber, S. Wiczorek, M. Wolfrum, "Excitability and self-pulsations near homoclinic bifurcations in semiconductor laser systems", *Optics Communications* vol. 215, pp. 367-379, 2003.
11. U. Bandelow, M. Radziunas, J. Sieber, M. Wolfrum, "Impact of Gain Dispersion on the Spatio-Temporal Dynamics of Multisection Lasers", *IEEE J. Quantum Electron.* **37**, pp. 183-188, 2001.
12. M. Radziunas, H.-J. Wünsche, B. Sartorius, O. Brox, D. Hoffmann, K. Schneider, D. Marcenac, "Modeling Self-pulsating DFB Lasers with an Integrated Phase Tuning Section", *IEEE J. Quantum Electron.* **36** pp. 1026-1034, 2000.
13. U. Bandelow, H. Wenzel and H.-J. Wünsche, "Influence of inhomogeneous injection on sidemode suppression in strongly coupled DFB semiconductor lasers", *Electronics Letters*, vol. 28, pp. 1324-25, 1992.
14. Yves Champagne and Nathalie McCarthy, "Influence of the axially varying quasi-Fermi-level separation of the active region on spatial hole burning in distributed-feedback semiconductor lasers", *Journal of Applied Physics* vol. 72, pp. 2110-2118, 1992.
15. P. G. Eliseev and A. E. Drakin, "Self-distribution of the current in laser diodes and its possible use for reducing the optical nonlinearity of the active medium", *Quantum Electronics* **26**, pp. 299-302, 1996.
16. P. G. Eliseev, A. G. Glebov, and M. Osinski, "Current self-distribution effect in diode lasers: analytic criterion and numerical study", *IEEE Journ. Select. Topics Quant. Electron.* vol. 3, pp. 499-506, 1997.
17. M. Radziunas, H.-J. Wünsche, O. Brox, F. Henneberger, "Excitability of a DFB laser with short external cavity", WIAS-Preprint No. 712, 2002, in: SPIE Proceedings Series, 4646, 2002, pp. 420-428.
18. M. Radziunas, H.-J. Wünsche; "Dynamics of multisection DFB semiconductor laser: traveling wave and mode approximation models", WIAS-Preprint No. 713, 2002, in: SPIE Proceedings Series, 4646, 2002, pp. 27-37.
19. H. Wenzel, U. Bandelow, H.-J. Wünsche and J. Rehberg, "Mechanisms of fast self pulsations in two-section DFB lasers", *IEEE J. Quantum Electron.*, vol. **32**, pp. 69-79, 1996.
20. V.Z. Tronciu, H.-J. Wünsche, J. Sieber, K. Schneider, F. Henneberger, "Dynamics of single mode semiconductor lasers with passive dispersive reflectors," *Optics Communications* 182, pp. 221228 (2000).